Journal of Coastal Research	19	1	1–11	West Palm Beach, Florida	Winter 2003

Diffusion Approach for Suspended Sand Transport Under Waves

Dang Huu Chung† and Leo C. Van Rijn‡

†GKSS Institute for Coastal Research
Max-Planck Str.
21502 Geesthacht, Germany
chung.dh@gkss.de

‡Delft Hydraulics
P.O. Box 177
2600 MH, Delft, The Netherlands
Leo.vanrijn@wldelft.nl

ABSTRACT

CHUNG, D.H. and VAN RIJN, L.C., 2003. Diffusion approach for suspended sand transport under waves. *Journal of Coastal Research*, 19(1), 1–11. West Palm Beach (Florida), ISSN 0749-0208.

The results of theoretical studies on suspended sand transport over a rippled bed under irregular waves are presented. The mathematical model is based on the classical diffusion approach, in which both the turbulence-related diffusion and the effective wave-related diffusion are taken into account. Although the model is less effective in accurately simulating the instantaneous sand concentrations, the time-averaged sand concentration can be reasonably well simulated in the ripple regime using the calibrated equations. In particular, the proposed formula for the coefficient of diffusion by waves considerably improved the predicted value of the time-averaged vertical distribution of suspended sediment concentration. The accuracy of prediction for the suspended sediment transport is dependent on the type of applied bed-boundary condition for the sand concentration. The measured reference concentration should be used as the boundary condition at the reference level for fine sand. Steep vortex ripples for coarse sand and relatively flat ripples for fine sand occurred. For low ripple steepness and large wave height, the computed wave-related suspended transports for both types of boundary condition are directed onshore, in line with the measured results. The wave-related suspended transport increases with wave height and decreases with sand size. Suspended sediment transport mainly occurs in the near-bed layer, with a thickness of from 10 to 20 times the ripple height. The position of measurement should be as close to the bed as possible (down to $z = 0.01$ m above the bed) to determine accurate values of the depth-integrated transport rate.

ADDITIONAL INDEX WORDS: *1DV model, rippled bed, vortex-induced mixing coefficient, wave-related sand transport.*

INTRODUCTION

The phenomenon of sediment transport in the surf zone is a complicated natural process. This problem attracts the attention of many researchers, with solutions involving both mathematical and physical models to achieve a better understanding of this process. The suspended sand transport rate in the surf zone comprises two major components: current-related and wave-related transport. The current-related transport component is considered to be the convective sand transport caused by the mean currents, such as tide-, wind- and wave-driven currents, in the presence of short (high-frequency) surface waves acting as stirring agents. The wave-related transport component is herein defined as the transport of sand particles by the oscillating (orbital) fluid motion due to high-frequency waves. Current-related transport over rippled beds has been studied in considerable detail (VAN RIJN *et al.*, 1993; VAN RIJN and HAVINGA, 1995), but wave-related transport is less well known. Both the magnitude and direction of wave-related transport vary depending on the geometry of the ripples; in particular, relatively flat ripples may result in onshore transport, whereas steep vortex-induced ripples may cause offshore transport due to phase differences between instantaneous fluid velocities and sand concentrations near the bed (GRASMEIJER and VAN RIJN, 1999; OSBORNE and GREENWOOD, 1992; OSBORNE and VINCENT, 1996; VAN RIJN *et al.*, 1993; VAN RIJN, 1998 and VINCENT and GREEN, 1990). Wave-related transport over a flat bed has been studied in more detail based on numerous experiments in wave flumes (see RIBBERINK, 1998, for an overview). Generally, wave-related transport over a flat bed is found to be onshore for sand larger than about 0.15 mm, because phase differences are less important in the thin sheet flow layer.

This paper is based largely on results from the 1DV model, which is a modified version of an existing model developed by RIBBERINK and AL-SALEM (1995). We included the effect of ripple-related sediment mixing and extended the model to conditions with irregular waves. Herein, the model will be used to study the wave-related suspended sand transport in the ripple regime under irregular waves and to demonstrate whether a diffusion-type model can be applied to simulate the suspension mechanism caused by ripple-induced vortices. The vortex-induced transport process may be a convective process related to the migrational behaviour of oscillating, coherent, ripple-induced vortices rather than a turbulence-induced diffusion process as pointed out by NIELSEN (1992).

00061 received 25 April 2000; accepted in revision 10 April 2002.

Table 1. *Measurement program.*

Data Set	Measurement No.	Number of Tests	Grain Size, d_{50}	Wave Height, H_s	Orientation of ASTM
I	A1,A1B,A2A, D1,D2,D3,D4,D5	8	0.33 mm	1.00 m	−90° −120°
II	B1A,B2A,B1B, E1,E2,E3,E4,E5	8	0.33 mm	1.25 m	−90° −120°
III	G1,G2,G3,G4, J1,J2,J3	7	0.16 mm	1.00 m	−120° −90°
IV	H1,H2,H3,H4,H5, K1,K2,K3,K4	9	0.16 mm	1.25 m	−120° −90°
V	M1,M2,M4	3	0.16 mm	1.50 m	90°

EXPERIMENTAL DESIGN

The experiments were carried out in the Delta Flume of Delft Hydraulics. This is a large-scale flume with a total length of 233 m, a depth of 7 m and a width of 5 m. On the bed a sand layer of 0.5 m was placed over a length of about 40 m. Regular and irregular waves were generated by a piston activated wave board on one side of the flume. The instruments for measurement were mounted on a tripod, which was placed on the sand bed at location x = 125 m. For each test the instruments were operated for about 15 min to sample over a representative wave record.

The following instruments were used in the flume:

- The two-dimensional, five-fold ASTM (Acoustical Sand Transport Meter) to measure the instantaneous concentration and velocity components at five different positions in the vertical direction. The ASTM frame was positioned on the sand bed.
- Two electromagnetic flow meters (EMF) in a vertical array and mounted on the flume wall to measure velocity.
- Two optical back-scatter sensors (OBS) to measure the instantaneous concentration at two positions.
- A pump sampling system (10 intake nozzles) also located along the flume wall (intake nozzles at about 0.3 m from the wall).
- A ripple profiler to measure bed form: The Sand Ripple Profiler is a 2-MHz scanning sonar system comprising a pencil-beam transducer on a rotating head. Thus for each head position a back-scatter profile can be obtained, allowing a 2D image through the water to be built up. Data is transferred to a PC via a serial link following capture using an on board 8-bit ADC.

Other instruments were also used in this experiment. During the first test series the sand bed had a d_{50} of 330 μm, and during the second test series d_{50} was 160 μm. The water depth was 4.5 m in all experiments.

The experimental conditions are presented in Table 1, including different sand sizes, wave types, wave heights and the orientation of the ASTM; the measurements are divided into five groups. The orientation of the ASTM was changed during the test program in order to observe the influence of measurement position on the results. The position of the sensors was altered so that they were not located in the plane of orbital motion (where the measurement volume is least disturbed by the sensors). In the field the direction of the waves cannot be controlled, and this may lead to an unfavourable orientation of the ASTM with respect to the plane of orbital motion.

MATHEMATICAL MODEL

A 1DV point model based on a numerical solution of the time-dependent sediment diffusion equation was used to simulate instantaneous sand concentrations. The model is a version of that presented by RIBBERINK and AL-SALEM (1995) modified to include the effects of irregular waves and vortex-related mixing. Most other researchers (*e.g.* JONSSON, 1963; KAJIURA, 1968; HORIKAWA and WATANABE, 1968; BAKKER, 1974; BREVIK, 1981; FREDSOE *et al.*, 1985; RAKHA *et al.*, 1997) have used similar models for plane bed conditions, with the exception of RAKHA *et al.* (1997), who applied their model to compute the profile evolution within a predominantly rippled surf zone.

The turbulent fluid movement for (horizontal) uniform flow in the vertical plane is considered assuming that the vertical velocity is relatively small compared to the horizontal velocity. Furthermore, it is assumed that the region of flow can be divided into an upper and a lower layer, in which the upper layer has no vertical velocity gradient. Hence, by using the pressure-gradient term from the equation for the upper layer, movement in the lower layer can be described by the Reynolds' equation as follows:

$$\frac{\partial u}{\partial t} = \frac{\partial u_0}{\partial t} + \frac{\partial}{\partial z}\left(\nu_t \frac{\partial u}{\partial z}\right), \qquad z_0 \le z \le h, \tag{1}$$

in which $u(z, t)$ = horizontal velocity in the oscillatory lower layer, h = depth, u_0 = horizontal velocity at elevation $z = h$ distinguishing between the lower and upper layers, t = time, z = elevation above bed, ν_t = turbulent viscosity and z_0 = position of zero velocity.

Eq. (1) is suitable for simulating the orbital flow field over a plane bed or a bed with relatively flat ripples and, therefore, no flow separation. It cannot simulate the detailed vortex motions over pronounced ripples, which is horizontally non-uniform. Since attention is focussed on the wave-related suspended transport, Eq. (1) is herein used to describe the general orbital motion and the turbulence-related mixing characteristics. The basic idea is to evaluate the performance of a fairly simple model with respect to the suspension characteristics over a rippled bed and to evaluate whether the model can be adjusted to produce accurate wave-related transport rates.

Prandtl's theory on mixing length is used as a turbulence closure for the equation and therefore the eddy viscosity is described by

$$\nu_t = \beta_1 l^2 \left|\frac{\partial u}{\partial z}\right|, \tag{2}$$

in which β_1 = eddy viscosity adjusting coefficient, l = mixing length; the latter is determined by Prandtl's formula:

$$l = \kappa z, \tag{3}$$

where κ = Von Karman constant ($\kappa = 0.4$).

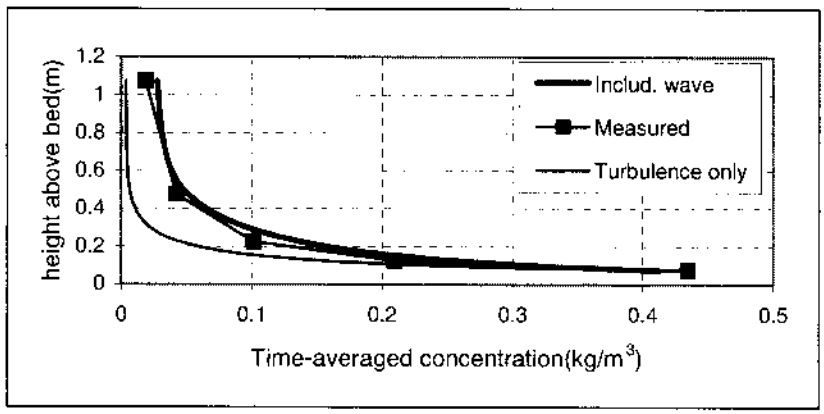

Figure 1. Time-averaged concentration profile with and without vortex (test G1).

The initial and boundary conditions used in the model are given in the following:

$$u(z, t)|_{z=h} = f_1(t), \tag{4}$$

$$u(z, t)|_{z=z_a} = 0, \tag{5}$$

in which $f_1(t)$ is a function determined empirically from a data record of irregular wave orbital velocity.

The initial condition is as follows:

$$u(z, t)|_{t=0} = f_2(z), \qquad z_0 \le z \le h, \tag{6}$$

in which $f_2(z)$ is a function of velocity. A hyperbolic tangent distribution is used for the initial velocity based on the value at $z = h$.

Using the same assumptions as for flow (Eq. 1), the vertical distribution of sediment concentration is described by the 1DV diffusion equation as follows:

$$\frac{\partial c}{\partial t} - \frac{\partial}{\partial z}(w - w_s)c = \frac{\partial}{\partial z}\left(\varepsilon_s \frac{\partial c}{\partial z}\right), \qquad z_a \le z \le h, \tag{7}$$

in which w = vertical flow velocity, w_s = the settling velocity of sediment particle, c = volume concentration, z_a = reference level, and ε_s = diffusion coefficient for sediment. The reference level is assumed to be equal to the effective bed roughness, k_s, which is assumed to be equal to the ripple height.

To represent additional vortex-related suspension process-

Table 2. *Input parameters for computations.*

Test	Time-avg. Velocity at $z = h$, U_m	Bed Roughness, k_s	Reference Level, z_a	Coeff., Eq. (16), m	Coeff., Eq. (10), n	Ripple Height, r	Ripple Length, λ	Ripple Steepness, r/λ
A1	0.031 m/s	0.06 m	0.06 m	0.5	12.0	0.06 m	0.22 m	0.27
D1	−0.005 m/s	0.06 m	0.06 m	0.5	12.0	0.06 m	0.22 m	0.27
D3	−0.005 m/s	0.06 m	0.06 m	0.5	12.0	0.06 m	0.22 m	0.27
B1A	−0.034 m/s	0.05 m	0.05 m	0.3	12.0	0.05 m	0.23 m	0.22
B2A	−0.034 m/s	0.05 m	0.05 m	0.3	12.0	0.05 m	0.23 m	0.22
B1B	0.036 m/s	0.05 m	0.05 m	0.3	12.0	0.05 m	0.23 m	0.22
E3	−0.018 m/s	0.05 m	0.05 m	0.3	12.0	0.05 m	0.23 m	0.22
E4	−0.010 m/s	0.05 m	0.05 m	0.3	12.0	0.05 m	0.23 m	0.22
E5	−0.010 m/s	0.05 m	0.05 m	0.3	12.0	0.05 m	0.23 m	0.22
G1	−0.038 m/s	0.03 m	0.03 m	0.05	38.0	0.03 m	0.72 m	0.04
G2	−0.018 m/s	0.03 m	0.03 m	0.05	38.0	0.03 m	0.72 m	0.04
G4	−0.022 m/s	0.02 m	0.03 m	0.05	38.0	0.03 m	0.72 m	0.04
J1	−0.031 m/s	0.03 m	0.03 m	0.05	38.0	0.03 m	0.72 m	0.04
J2	−0.032 m/s	0.03 m	0.03 m	0.05	38.0	0.03 m	0.72 m	0.04
J3	−0.031 m/s	0.03 m	0.03 m	0.05	38.0	0.03 m	0.72 m	0.04
H2	−0.038 m/s	0.03 m	0.03 m	0.05	38.0	0.03 m	0.72 m	0.04
H3	−0.037 m/s	0.03 m	0.03 m	0.05	38.0	0.03 m	0.72 m	0.04
H4	0.026 m/s	0.03 m	0.03 m	0.05	38.0	0.03 m	0.72 m	0.04
H5	0.034 m/s	0.03 m	0.03 m	0.05	38.0	0.03 m	0.72 m	0.04
K2	0.030 m/s	0.03 m	0.03 m	0.05	38.0	0.03 m	0.72 m	0.04
K4	−0.036 m/s	0.03 m	0.03 m	0.05	38.0	0.03 m	0.72 m	0.04
M1	−0.044 m/s	0.02 m	0.02 m	0.05	38.0	0.02 m	0.72 m	0.03
M2	−0.032 m/s	0.02 m	0.02 m	0.05	38.0	0.02 m	0.72 m	0.03
M4	−0.030 m/s	0.02 m	0.02 m	0.05	38.0	0.02 m	0.72 m	0.03

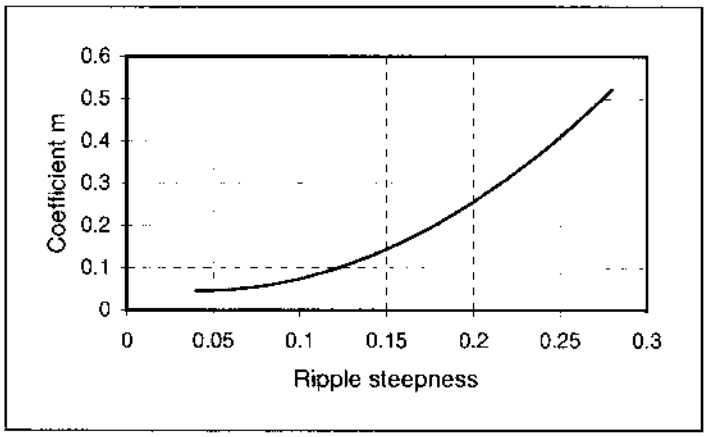

Figure 2. Relation between ripple steepness and coefficient m.

es, the overall sediment mixing coefficient was modelled as the sum of two components, the bottom-induced turbulence and the effective vortex-induced mixing:

$$\varepsilon_s = \sqrt{\varepsilon_{st}^2 + \varepsilon_{sw}^2} \tag{8}$$

in which ε_{st}, ε_{sw} are the mixing coefficients for sediment due to turbulence and due to vortex motions, respectively. The turbulence-related sediment mixing coefficient is related to the eddy viscosity, ν_t, by the coefficient β_2:

$$\varepsilon_{st} = \beta_2 \nu_t. \tag{9}$$

Eq. (9) represents the effect of discrete sediment particles on the diffusion process; basically, turbulent viscosity applies to the diffusion of momentum. So this equation is fully correct for the diffusion of discrete particles in the more or less homogeneous turbulence present in an oscillatory flow over a flat bed. With ripples, strong regular vortices are generated close to the bed. These vortices cause a perturbation of the 'normal' turbulence field. This has been represented by an additional vortex-related diffusion coefficient. That is supposed to be dominant close to the bed. The value of β_2 is not well known; values smaller and larger than 1 have been used (see VAN RIJN, 1993). Herein, $\beta_2 = 1$ is used.

The vortex-induced mixing is supposed to be described by

$$\varepsilon_{sw} = \frac{1}{n}\hat{U}z\left(1 - \frac{z}{h}\right). \tag{10}$$

Eq. (10) is based on dimensional analysis and assumes that the sand concentration profile is of the hyperbolic type, $c \sim (h/z - 1)^n$, with n being a calibration coefficient most likely dependant on grain size and ripple dimensions. Furthermore, it is assumed that peak orbital velocities ($\hat{U}$) are dominant in driving the vortices. The peak orbital velocity is described by

$$\hat{U} = \frac{1}{2}(U_{on}(z, T) + U_{off}(z, T))\big|_{z=h}, \tag{11}$$

in which U_{on} and U_{off} are onshore and offshore peak values of orbital velocity in the case of irregular waves, respectively, and T is the wave period. The effective vortex-induced mixing was determined by calibration of the coefficient n in Eq. (10) through the comparison of the measured and computed time-averaged sand concentrations.

The boundary equations for the sediment diffusion equation are as follows:

The initial condition is

$$c(z, t)\big|_{t=0} = f_3(z), \qquad z_a \le z \le h, \tag{12}$$

in which f_3 is a function derived from measured data.

The boundary condition at $z = h$ is

$$\varepsilon_s \frac{\partial c}{\partial z} = -w_s c, \qquad z = h. \tag{13}$$

The boundary condition at $z = z_a$ is

$$c(z, t)\big|_{z=z_a} = c_a(t) \qquad \text{at } z = z_a \quad \text{or} \tag{14}$$

$$\varepsilon_s \frac{\partial c}{\partial z} = -w_s c_a, \quad \text{at } z = z_a, \tag{15}$$

in which c_a = suspended sand concentration at the reference level and is given from either a proposed formula or measured instantaneous values.

The applied c_a expression reads

$$c_a = m\rho_s \frac{(\theta' - \theta'_{cr})^{1.5}}{D^*}, \tag{16}$$

in which θ' = instantaneous dimensionless bed shear stress related to the grains; θ'_{cr} = critical dimensionless bed shear stress, known as Shields parameter; ρ_s = density of sediment; D^* = dimensionless particle diameter; and m = empirical coefficient (calibration) related to ripple characteristics. Ripple height and length are defined as r and λ, respectively.

CALIBRATION OF THE MODEL AND NUMERICAL SOLUTIONS

The finite difference method, based on the implicit scheme of Crank-Nicolson, was used to solve Eqs (1) and (4)–(6) for horizontal velocity, and the implicit upwind scheme was used

in Eqs (7) and (12)–(14) to find vertical distribution of sediment concentration. It should be noted that the grids for flow and sediment diffusion equations are different and that a staggered grid with smaller grid size near the bed was used for more accurate and stable computation results. The data sets and basic input values of the model are given in Tables 1 and 2, which include the d_{50} of the bed, constant fall velocity of suspended sand, w_s (based on settling tests using suspended sediment samples), and effective bed roughness, k_s, which is assumed to be equal to the measured ripple height.

The calibration of the vortex-related mixing coefficient is based on the fitting of measured and computed time-averaged sand concentrations. It is shown in Figure 1 that the time-averaged sand concentration is much too small when only the turbulence-related mixing coefficient is used. The fact that the calculated concentration is consistently lower than the observed concentration indicates that the turbulent eddy viscosity in the model is lower than the true effective viscosity. Introducing a vortex-related mixing coefficient as determined by Eq. (10) improved the vertical distribution of sediment concentration considerably compared to the measurement results, and similar results were obtained for all other tests. Under the action of bottom-induced turbulent mixing only, the suspended sediment concentration is highest near the bed and decreases quickly upward. Of the 35 test results, 24 of the time-averaged sand concentrations (DANG HUU and GRASMEIJER, 1999) were used to determine the n-coefficient of the vortex-related mixing coefficient and the m-coefficient of the reference concentration expression by fitting the measured and computed time-averaged concentrations (Table 2).

The n-coefficient was found to depend on the grain size of the bed material: $n = 12$ for coarse sand of 0.33 mm ($w_s = 0.03$ ms $^{-1}$), and $n = 38$ for finer sand of 0.16 mm ($w_s = 0.011$ ms^{-1}). A smaller n-value implies stronger vortex-related mixing, which seems realistic because the ripples were more pronounced (steep vortex ripples with $r/\lambda = 0.27$) in the tests with a coarse sand bed of 0.33 mm.

The m-coefficient was found to be related to the ripple steepness (r/λ), with m-values in the range of $m = 0.05$ for $r/\lambda = 0.04$ to $m = 0.27$ for $r/\lambda = 0.5$. The results can be represented by (see Figure 2)

$$m = 8.4\left(\frac{r}{\lambda}\right)^2 - 0.7\frac{r}{\lambda} + 0.06. \quad (17)$$

Instantaneous velocities and concentrations measured and computed at 4 elevations (0.075, 0.125, 0.225 and 0.475 m) for a typical test (test G1) are shown in Figure 3a and b. The measured velocities at $z = 1.075$ m are used as the upper boundary condition of the model, so the comparison at this elevation is not presented. The sand concentrations at the lower boundary condition of $z = z = 0.075$ m are taken from measured concentrations as well as from Eq. (16). Based on these conditions, the model computations show quite good results for the concentration at the lower elevations and for the orbital velocity at the higher elevations (close to the boundaries). Further away from the boundaries, the discrepancy between computed and measured values gradually increases. The computed instantaneous results at positions near the bed based on the measured reference concentration are also shown to be much better than those based on Eq. (16). Furthermore, the computed instantaneous concentrations shows less oscillation than the measured concentrations. This latter effect results in less-accurate predictions of the wave-related sediment transport rate, as will be shown later. The vertical distribution of the time-averaged sand concentrations is not strongly affected by the type of boundary condition (measured data or Eq. 16), as shown in Figure 4.

For all cases under consideration the computed instantaneous velocities outside the layer affected by the ripples (roughly two ripple heights above the mean bed; $z > 0.1$ to 0.2 m) behave quite well in comparison with the measured velocities. The vertical distribution of the time-averaged velocities is shown in Figure 4. Considerable errors occur close to the bed in the vicinity of the ripples ($z < 0.1$ m).

Figure 5 shows computed and measured time-averaged velocity profiles for the 24 tests considered in terms of mean values (and standard error range) for each of the 5 data sets. Figure 6 shows similar results for the time-averaged sand concentrations. The time-averaged sand concentrations at higher elevations ($z > 0.5$ m) are largest for data set V, with the largest significant wave height and the finer sand of 0.16 mm, whereas the near-bed concentrations are largest for the case with steep vortex ripples (data sets I and II). These results show that a diffusion-type model is adequate in simulating the time-averaged sand concentration distribution, provided that the vortex-related suspension mechanism is modelled using an effective mixing coefficient. The discrepancies of time-averaged concentration between using Eq. (16) and the measured data for reference concentrations are quite small. As regards the standard errors of both the computed and measured results, the standard errors of the velocities change significantly for each test due to the presence of the ripples, while the standard errors for concentration are quite small and more stable at the same levels.

EVALUATION OF WAVE-RELATED SUSPENDED TRANSPORT RATES

The instantaneous velocity and concentration are defined as the sum of the time-averaged component and the wave-related oscillations as follows:

$$u(z, t) = \bar{u}(z) + \tilde{U}(z, t), \quad (18)$$

$$c(z, t) = \bar{c}(z) + \tilde{C}(z, t). \quad (19)$$

The components due to high and low frequencies are not presented separately here. The wave-related suspended sediment transport rate is defined as follows:

$$Q_w \equiv \overline{(u - \bar{u})(c - \bar{c})} = \overline{u \cdot c} - \bar{u} \cdot \bar{c}, \quad (20)$$

Equation (20) is applied to each computation result corresponding to the tests in Table 2. Comparison with the data shows that the computed wave-related transport rates close to the bed are not accurate when the reference concentration is computed by a bed-shear-stress-related expression. The model results are better if the measured sand concentrations at the lowest point are used as a boundary condition for the fine sand bed of 0.16 mm. However, the predicted reference

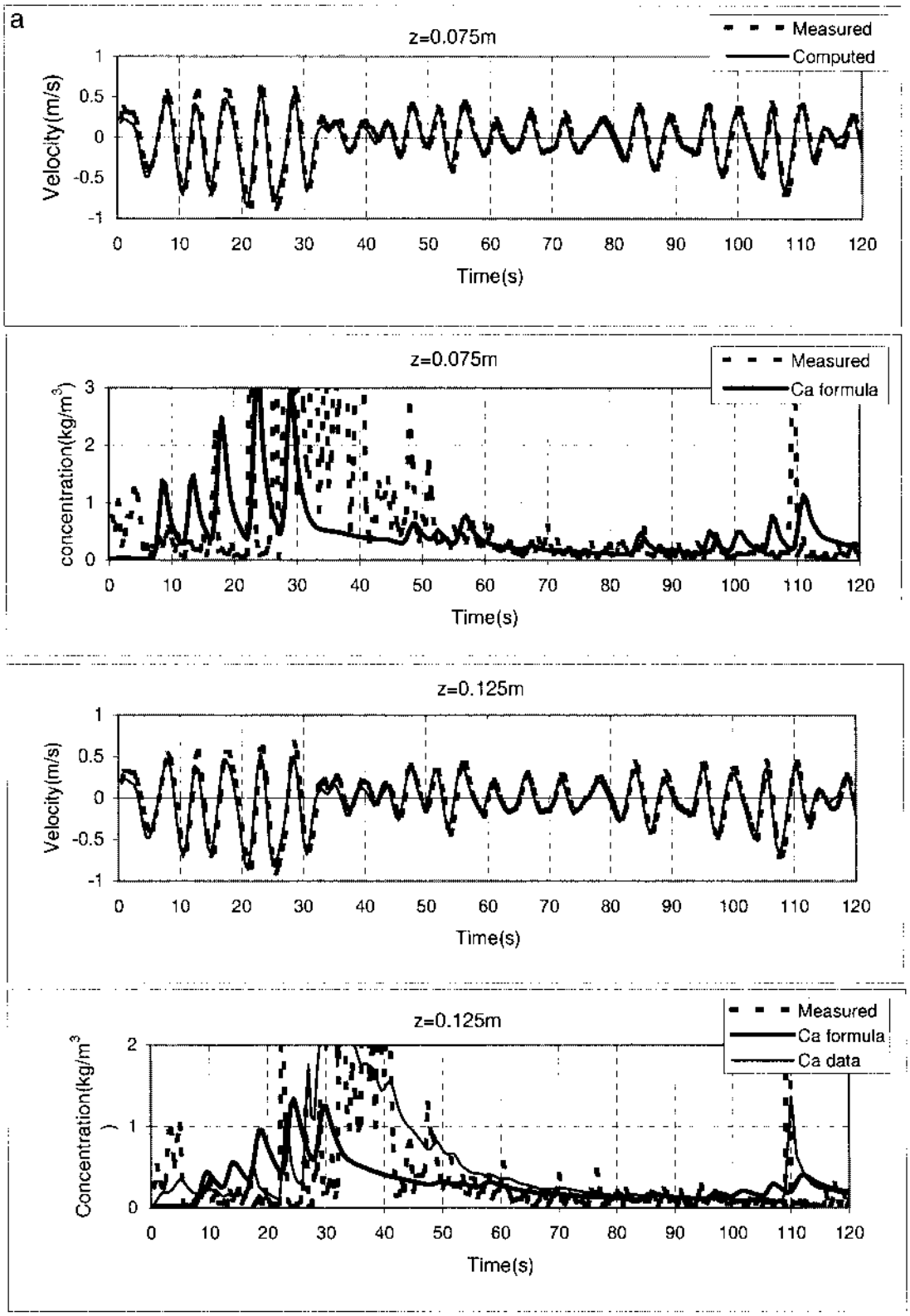

Figure 3a. Instantaneous velocity and concentration at two elevations, $z = 0.075$ and 0.125 m for test G1.

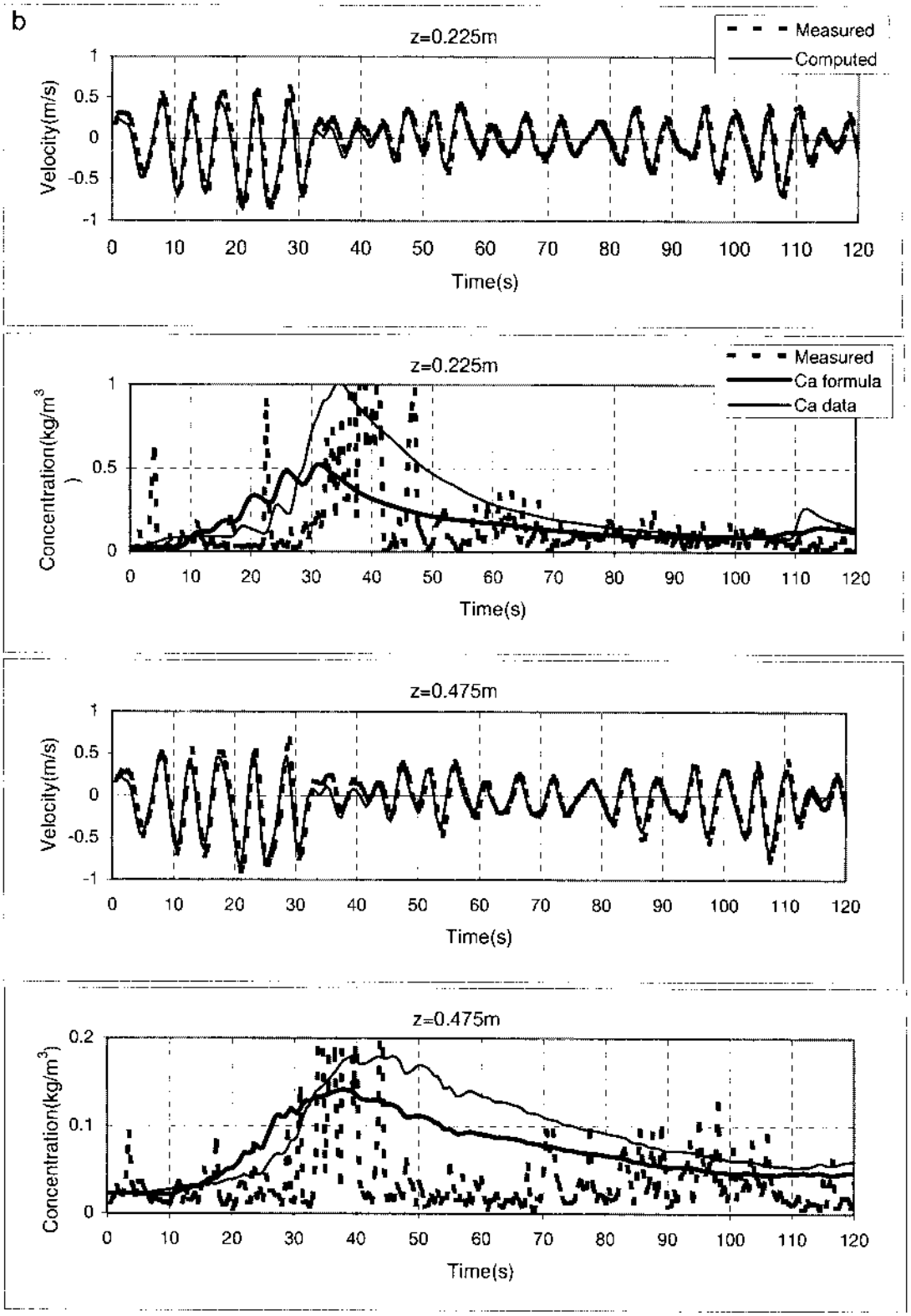

Figure 3b. Instantaneous velocity and concentration at two elevations z = 0.225 and 0.475 m for test G1.

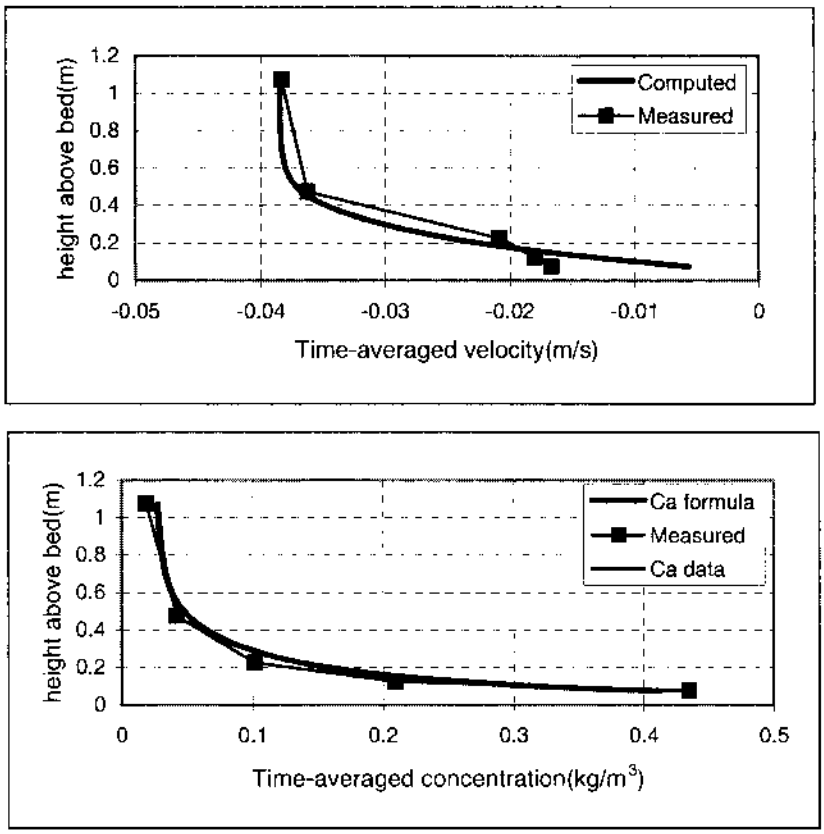

Figure 4. Computed and measured time-averaged velocity and concentration profiles for test G1.

concentration yields better results for coarse sand of 0.33 mm. This can also be observed in Figure 7, which presents the computed depth-integrated transport rates (between the lowest, $z = 0.075$ m and the highest measurement point, $z = 1.075$ m) versus measured depth-integrated transport rates (between the same points). For fine sand and large wave height (data set V) the computed wave-related sand transports with two types of reference concentration are onshore, in line with the measured values. The dashed lines represent an absolute error of 0.01 kg m^{-1} s^{-1}.

There is a range of causes for the discrepancies between measured and computed wave-related suspended transport rates. As seen in Figures 3a and b, the computed instantaneous concentrations do not agree well with the measured values, although the time-averaged values are quite good. This problem is related to the geometry of the ripples and to the dynamics of entrainment and transportation of sediment particles from the rippled bed into the flow. It appears that the instantaneous behaviour of the vortices and associated sand concentrations cannot be represented sufficiently by a diffusion-type model. Moreover, the interaction between sediment and fluid particles is not considered in the present model. The changes of fluid density and turbulence due to the presence of high near-bed sand concentrations may influence the dynamic process of flow and sediment transport.

DISCUSSION AND CONCLUSIONS

Ripple steepness is a very important factor, because it determines the scale of bed roughness (HITCHING and LEWIS, 1999) and hence has a strong influence on the vertical distribution of horizontal flow velocity and sand concentration. As the precise measurement location with respect to the ripple crest is unknown for these Delta flume experiments, many repetitive measurements have been made to ensure representative sampling at various locations along the migrating ripples. Thus, the measured mean profiles of Figure 5 represent a range of spatially-averaged (over a ripple length) mean velocity profiles. The error ranges give an indication of the horizontal variability involved. A comparison of measured and computed fluid velocities for 0.33 mm sand (Figure 5) shows that a simple 1DV model cannot be used to determine accurate values of the mean currents very close to steep ripples. Somewhat better results are obtained for data sets II and IV for 0.16 mm sand with flat ripples using an effective bed roughness equal to the ripple height. Accurate simulation of the flow field near a rippled bed basically requires the application of a 2DV model in combination with a higher-order turbulence closure (k ε method) or direct large-scale eddy simulation (LES method), which is beyond the scope of the present study.

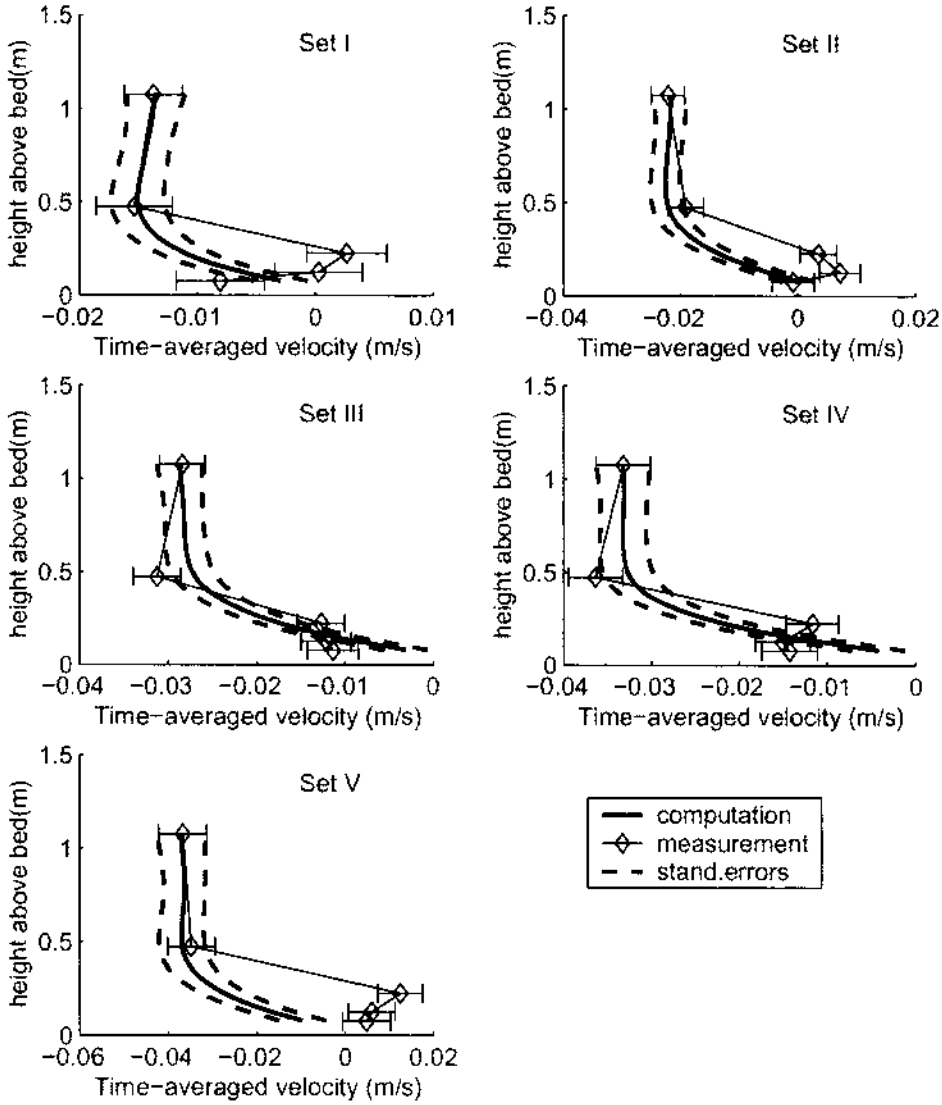

Figure 5. Time-averaged velocities for combined tests.

The time-averaged sand concentrations can be reasonably well simulated for both sand sizes using the classical diffusion approach, provided that the reference concentration near the bed is modelled with sufficient accuracy and that the vortex-related mixing characteristics are taken into account (calibration). Neglecting the vortex-related mixing coefficient yields time-averaged sand concentrations that are much too small (Figure 1). Further research is necessary to relate the reference concentration and the vortex-related mixing coefficient to relevant hydrodynamic, sediment and bed-form parameters.

The measured instantaneous sand concentrations cannot be simulated very accurately using a relatively simple reference concentration based on instantaneous bed-shear stress only; the effect of ripple geometry has to be included to represent all sand- concentration peaks near the bed. The computed instantaneous sand concentrations at various elevations away from the bed show better agreement when measured data are used as a bed boundary condition. For all cases the computed instantaneous sand concentrations show less oscillations than the measured data, which is an indication that the diffusion approach is not fully capable of simulating the instantaneous processes. However, this does not seem to greatly affect the accuracy of the time-averaged sand concentrations, and hence the current-related transport, but it is of major importance for the wave-related suspended transport processes. The latter cannot be simulated very accurately by the present 1DV model in the case of a rippled bed, especially when the reference concentration is not accurately modelled.

For all cases the measured wave-related suspended transport is directed onshore, whereas current-related suspended transport is directed offshore, similar to time-averaged transport components.

The results of the present study for sand transport over

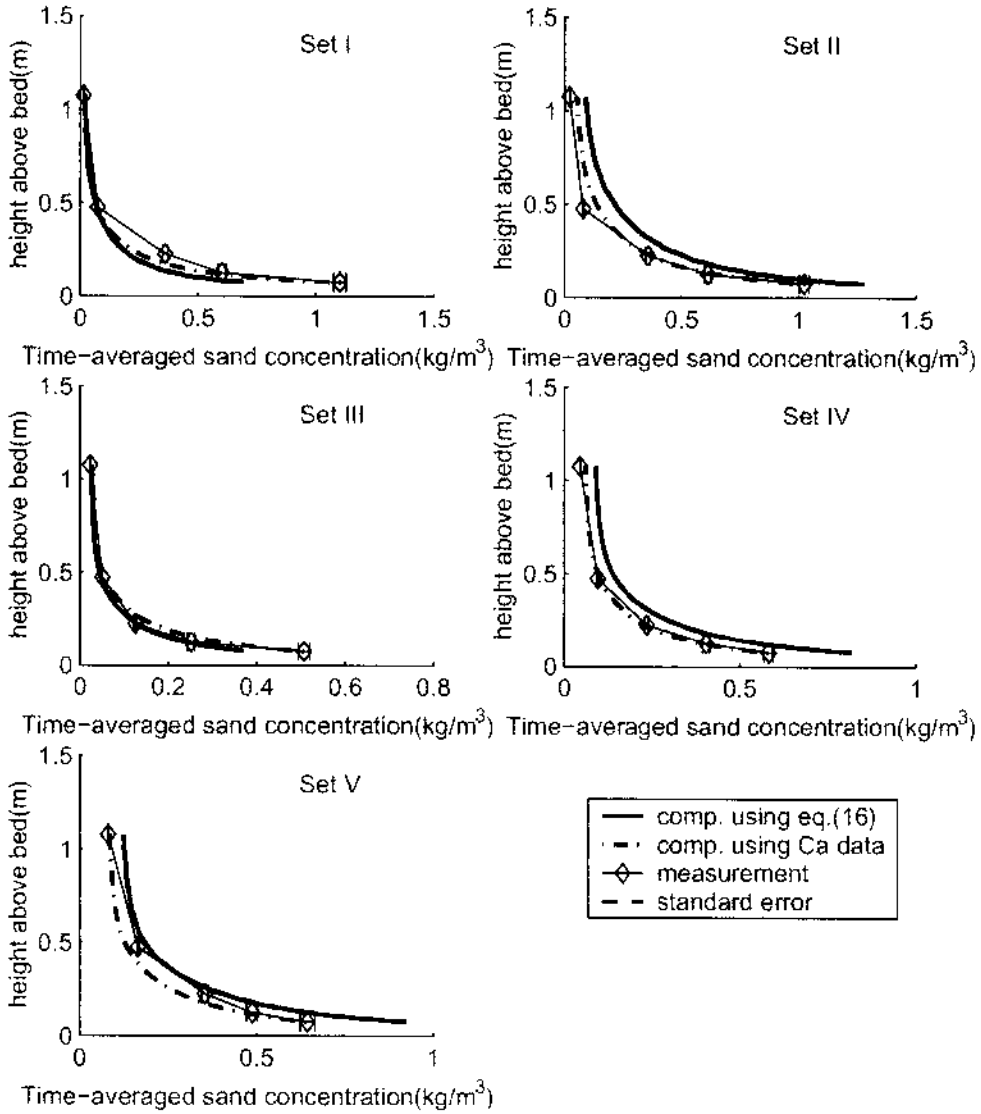

Figure 6. Time-averaged sand concentrations for combined tests.

beds of 0.16 mm and 0.33 mm sand under irregular waves can be summarised as follows:

(1) Ripple geometry is strongly affected by the bed-material characteristics: steep vortex ripples with $r/\lambda = 0.22$ to 0.27 occur for 0.33 mm sand (data sets I and II, see Table 1) and relatively flat ripples with $r/\lambda = 0.04$ occur for 0.16 mm sand (data sets III, IV and V).

(2) Suspended sediment transport mainly occurs in the near-bed layer with a thickness of about 0.3 to 0.5 m (water depth of 4.55 m), which is roughly equivalent to 10 to 20 times the ripple height.

(3) The measured wave-related suspended transport is directed onshore, whereas the current-related suspended transport is directed offshore, similar to time-averaged transport components.

(4) The onshore wave-related suspended transport increases with wave height ($H_{1/3}$ between 1 and 1.5 m) and decreases with sand size; the latter effect is related to the effect of decreasing ripple steepness and hence less-strong vortex motions for decreasing sand size.

(5) The instantaneous velocities and sand concentrations should be measured in points down to $z = 0.01$ m above the bed (if possible) to determine accurate values of the depth-integrated high-frequency transport rate.

(6) Although the 1DV model based on the classical diffusion approach cannot accurately simulate the instantaneous sand concentrations, it showed good ability in simulating the time-averaged suspended sand concentrations and hence the current-related suspended transport in the ripple regime, provided the reference concentration near the bed and the vortex-related mixing are represented with sufficient accuracy; both parameters are strongly related to the ripple characteristics.

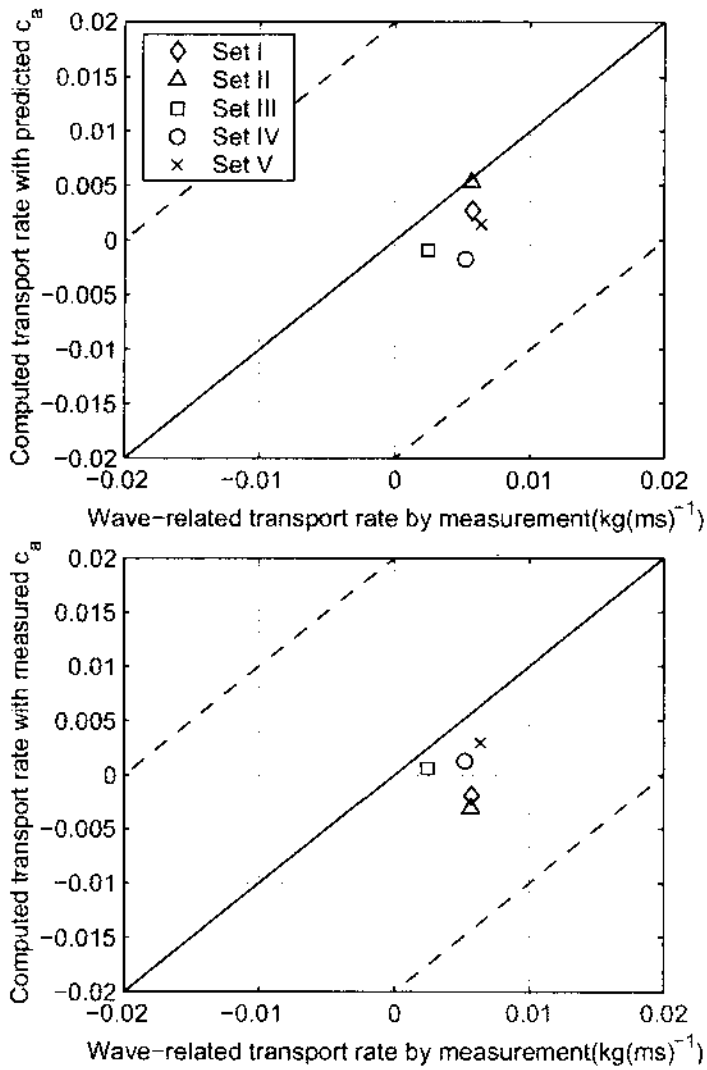

Figure 7. Computed versus measured (depth-integrated) wave-related transport rates.

ACKNOWLEDGMENTS

The experiments were conducted in the Delta flume of Delft Hydraulics under the framework of the LIP-program of the European Commission. This paper is also a part of works carried out in the frame of the Scholarship program of Utrecht University; the first author has been awarded such a scholarship. At the same time this publication is also funded by the Council for Natural Sciences of Vietnam.

LITERATURE CITED

BAKKER,W.T.,1974. Sand concentration in oscillatory. *Proceedings of the 14th International Conference on Coastal Engineering* (Copenhagen, ASCE), pp. 1129–1148.

BREVIK, I., 1981. Oscillatory rough turbulent boundary layers. *ASCE WW3,* 107, 175–188.

DANG HUU, C. and GRASMEIJER, B.T., 1999. Analysis of sand transport under regular and irregular waves in large-scale wave flume. Utrecht: University of Utrecht, Department of Physical Geography, *IMAU, Report R99-05,* 85p.

FREDSOE, J.; ANDERSEN, O.H., and SILBERG, S., 1985. Distribution of suspended sediment in large waves. *Journal of Waterway, Port, Coastal and Ocean Engineering,* 111(6), 1041–1059.

GRASMEIJER, B.T. and VAN RIJN,L.C., 1999. Transport of fine sands by currents and waves III: Breaking waves over barred profile with ripples. *Journal of Waterway, Port, Coastal and Ocean Engineering,* 125(2), 71–79.

HITCHING, E. and LEWIS, A.W., 1999. Bed roughness over vortex ripples. *Proceedings of the 4th International Symposium on Coastal Engineering and Coastal Sediment Processes* (Long Island, New York, ASCE), pp. 18–30.

HORIKAWA, K. and WATANABE, A., 1968. Laboratory study on oscillatory boundary layer flow. *Proceedings of the 11th Coastal Engineering Conference,* pp.467–486.

JONSSON, I.G., 1963. Measurements in the turbulent wave boundary layer. *Proceedings of the 10th Congress IAHR,* pp. 85–92.

KAJIURA, K., 1968. A model of the bottom boundary layer in water waves. *Bull. Earthquake Res. Inst,* 46, 75–123.

NIELSEN, P.,1992. *Coastal Bottom Boundary Layers and Sediment Transport.* New York: World Scientific, 324p.

OSBORNE, P.D. and GREENWOOD, B.G., 1992. Frequency-dependent cross-shore suspended sediment transport 2: A barred shoreface. *Marine Geology,* 106, 25–51.

OSBORNE, P.D. and VINCENT, C.E., 1996. Vertical and horizontal structure in suspended sand concentrations and wave-induced fluxes over bed forms. *Marine Geology,* 131, 195–208.

RAKHA, K.A.; DEIGAARD, R., and BROKER, I., 1997. A Phase-resolving cross-shore sediment transport model for beach profile evolution. *Coastal Engineering,* 31, 231–261.

RIBBERINK, J.S., 1998. Bed-load transport for steady flows and unsteady oscillatory flows. *Coastal Engineering,* 34, 59–82.

RIBBERINK, J.S. and AL-SALEM, A.,1995. Sheet flow and suspension of sand in oscillatory boundary layers. *Coastal Engineering,* 25, 205–225.

VAN RIJN, L.C. 1993. *Principles of Sediment Transport in Rivers, Estuaries and Coastal Seas.* Amsterdam: Aqua Publications, 730p.

VAN RIJN, L.C., 1998. *Principles of Coastal Morphology.* Amsterdam: Aqua Publications, 750p.

VAN RIJN, L.C. *et al.,* 1993. Transport of fine sands by currents and waves I. *Journal of Waterway, Port, Coastal and Ocean Engineering,* 119(2), 123–143.

VAN RIJN, L.C. and HAVINGA, F.J., 1995. Transport of fine sands by currents and waves II. *Journal of Waterway, Port, Coastal and Ocean Engineering,* 121(2), 123–133.

VINCENT, C.E and GREEN, M.O., 1990. Field measurements of the suspended sand concentration profiles and fluxes and of the resuspension coefficient over a rippled bed. *Journal of Geophysical Research,* 95(C7), 11591–11601.